Inorganic Chemistry

Article

pubs.acs.org/IC

Magnetic Anisotropy in Functionalized Bipyridyl Cryptates

Elisabeth Kreidt,[†] Caroline Bischof,[‡] Carlos Platas-Iglesias,*[,§] and Michael Seitz*[,†]

[†]Institute of Inorganic Chemistry, University of Tübingen, Auf der Morgenstelle 18, 72076 Tübingen, Germany

[‡]Inorganic Chemistry I, Ruhr-University Bochum, 44780 Bochum, Germany

[§]Departamento de Química Fundamental, Universidade da Coruña, Campus da Zapateira-Rúa da Fraga 10, 15008 A Coruña, Spain

Supporting Information

ABSTRACT: The magnetic properties of molecular lanthanoid complexes are very important for a variety of scientific and technological applications, with the unique magnetic anisotropy being one of the most important features. In this context, a very rigid tris(bipyridine) cryptand was synthesized with a primary amine functionality for future bioconjugation. The magnetic anisotropy was investigated for the corresponding paramagnetic ytterbium cryptate. With the use of a combination of density functional theory calculations and lanthanoid-induced NMR shift analysis, the magnetic susceptibility tensor was determined and compared to the unfunctionalized cryptate analogue. The size and orientation of the axial and rhombic tensor components show remarkably great resilience toward the decrease of local symmetry around the metal and anion exchange in the inner coordination sphere. In addition, the functionalized ytterbium cryptate also exhibits efficient near-IR luminescence.

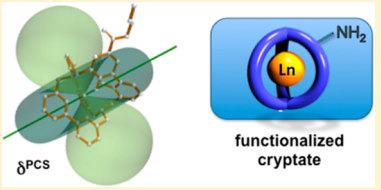

INTRODUCTION

The highly interesting physical properties of trivalent lanthanoids have made them crucial components in innovative scientific and technological applications.[1] One of the most prominent features in this respect is their unique magnetism, which has been used in many different areas such as NMR shift reagents,[2] magnetic resonance imaging contrast agents,[3] single-molecule magnets,[4] or paramagnetic tags in the structural biology of proteins.[5] One of the centrally important aspects of lanthanoid magnetism is its often very pronounced and well-defined anisotropy in the case of nonspherical f-electron distributions, that is, for all paramagnetic Ln^{3+} except Gd^{3+}. In general, the magnitude and the spatial dependence of the effects in molecular complexes are often very sensitive to the composition and the symmetry of the inner coordination sphere around the lanthanoid and the corresponding ligand field splitting of the f-orbitals. Consequently, ligand architectures that are able to provide a well-defined, unchanging coordination environment would be the best choice if time-invariant and predictable magnetic anisotropy is required. By far the most prevalent ligand class for lanthanoid complexation is based on 1,4,7,10-tetraazacyclododecane-1,4,7,10-tetraacetic acid (DOTA) and related systems.[6] Despite the great success of DOTA in fields related to lanthanoid magnetism, many DOTA-derived lanthanoid complexes often exhibit typical exchange processes that inherently affect magnetic anisotropy, for example, configurational exchange between Δ and Λ stereoisomers through rotation of the pendant arms and conformational flexibility associated with the inversion of the macrocyclic unit, which leads to interconversion between the square-antiprismatic and twisted square-antiprismatic geometries.[7] Some of these problems have been overcome with special ligand modifications[8] but remain a ubiquitous detrimental phenomenon overall. In addition, recent studies point to somewhat unpredictable magnetic behavior even in DOTA complexes with supposedly high symmetry[9] and the extreme sensitivity of the anisotropy toward exchange of additional, axially coordinated ligands such as H_2O or fluoride.[10] One of the alternatives to DOTA-derived ligand systems for lanthanoid chelation are tris(2,2′-bpy)-based cryptands (2,2′-bpy = 2,2′-bipyrdine) that have proven to be very valuable tools for bioanalytical luminescence applications.[11] Originally, they were introduced by Lehn et al. in the form of the flexible cryptates **1-Ln** (Figure 1).[12] Later development has shown the *N*,*N*′-dioxide analogues **2-Ln** to be conformationally and configurationally very stable on the NMR time scale, without any signs of the detrimental exchange processes typically observed for DOTA derivatives.[13]

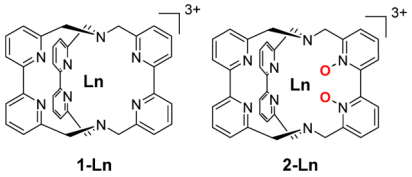

Figure 1. 2,2′-Bipyridine-based cryptate scaffolds. Flexible **1-Ln**[12] vs extremely rigid **2-Ln**.[13]

Despite the great potential that cryptates of the type **2-Ln** have in this area, this class of ligands is virtually absent from the field of lanthanoid magnetism. One of the major reasons for this phenomenon is the somewhat underdeveloped and sometimes cumbersome synthethic chemistry of cryptands, in

Received: March 8, 2016

DOI: 10.1021/acs.inorgchem.6b00591
Inorg. Chem. XXXX, XXX, XXX−XXX

contrast to the very mature synthetic methodology for the preparation of tailor-made DOTA-derivatives. Especially detrimental in this regard is the lack of cryptands with well-behaved and stable magnetic anisotropy that also have the possibility for covalent attachment via suitable, peripheral functional groups to other chemical entities such as proteins. In the past, there have been reports of a few monofunctionalized lanthanoid cryptates such as cryptates **3-Ln**[14] with a peripheral ester group or **4-Ln**[15] with a primary amine functionality for bioconjugation (Figure 2, top row). Unfortunately, these species are rather flexible and undergo the same unwanted exchange processes as seen in DOTA.

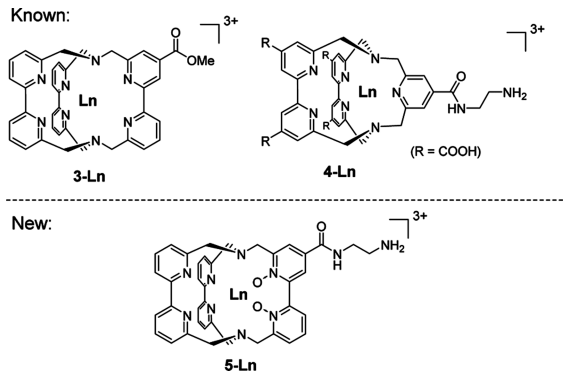

Figure 2. (top) Monofunctionalized lanthanoid cryptates **3-Ln**[14] and **4-Ln**.[15] (bottom) Rigid, monofuntionalized lanthanoid cryptate **5-Ln** developed for this study.

In this study, we alleviate this problem with the introduction of a new, monofunctionalized cryptate **5-Ln** (Figure 2, bottom) that is synthetically accessible on larger scales. For the corresponding ytterbium cryptate **5-Yb**, we investigate the influence that the functionalization and the concomitant reduction from C_2 to C_1 symmetry has on the magnetic anisotropy and the photoluminescence properties.

RESULTS AND DISCUSSION

Cryptate Design–Functionalization Strategy. The specific placement and the nature of the peripheral functional group onto the parent cryptate scaffold **2-Ln** is of crucial importance for achieving well-defined and stable complexes. First, functionalization in the 4-position on a pyridine unit is generally the most accessible from a synthetic perspective and points away from the metal binding site, therefore avoiding steric interferences with the nature of the core cryptate geometry (Figure 3). Second, our choice for the functional group fell on carboxylic acid derivatives (X in Figure 3) because of literature precedence (cf. **3-Ln** in Figure 2) and because of the great synthetic versatility of this motif for further modification/conjugation. Third and most importantly, the functionalization must be located on the 2,2′-bpy-*N*,*N*′-dioxide moiety (Figure 3, path B) and not on any of the pyridines of the 2,2′-bpy units (Figure 3, path A) to avoid the potential formation of diastereomeric cryptate species. Unfunctionalized cryptates like **2-Ln** already possess one stereogenic element in the form of the fixed helical arrangement of the biaryl moieties. Cryptates **6-Ln** (Figure 3) with the peripheral group on the bipyridines would feature a new and rather unusual stereogenic element due to the special topology of the macrobicyclic cryptand framework (Figure 4), which in turn would lead to the

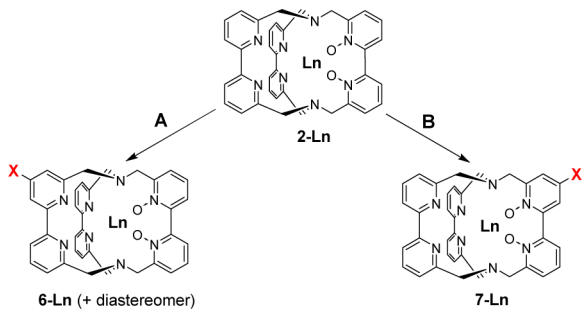

Figure 3. Possibilities for the introduction of the peripheral group X in the cryptate **2-Ln**. Path A: Functionalization at the 2,2′-bpy unit; Path B: Functionalization on the 2,2′-bpy-*N*,*N*′-dioxide moiety.

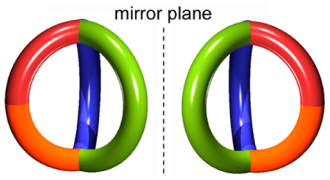

Figure 4. Unusual stereogenic element in cryptates **6-Ln** due to the topology of the macrobicyclic cryptand framework (the colors indicate the fact that all three cryptate arms are different and one is unsymmetric).

potential formation of diastereomeric cryptands. The diastereomers of the corresponding paramagnetic lanthanoid complexes would certainly have very different magnetic anisotropies which would, of course, completely defeat the purpose outlined in the introduction. The cryptates **7-Ln** do not suffer from this problem and are therefore ideal candidates for this study.

Cryptate Synthesis. The key building block for the synthesis of the cryptates **5-Ln** is the funtionalized 2,2′-bipyridine derivative **10** (Scheme 1), which is known to be

Scheme 1. Synthesis of Sodium Cryptate 15

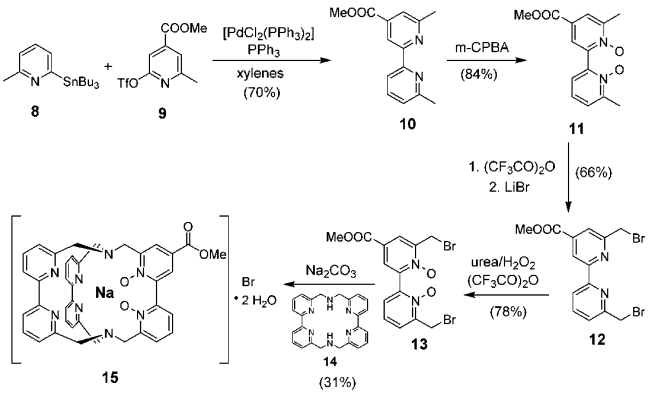

accessible by either Stille[16] or Negishi[14] cross coupling. Both reported procedures rely on chromatographic purification of **10**, which makes its preparation rather cumbersome on larger scales. We were therefore interested in developing an improved purification protocol that avoids chromatography. Our optimized approach utilizes the known Stille coupling[16] of tin precursor **8** and triflate **9** (Scheme 1). After the reaction, product **10** can conveniently be isolated in analytically pure form by a continuous liquid–liquid extraction using *n*-heptane and CH_3CN as the two liquid phases. So far, we successfully validated this protocol on scales of up to 80 mmol of starting

DOI: 10.1021/acs.inorgchem.6b00591
Inorg. Chem. XXXX, XXX, XXX–XXX

materials (**8** and **9**) giving product **10** in rather large amounts (>13 g). The subsequent reactions to sodium cryptate **15** are straightforward and start with the oxidation of **10** to the corresponding *N*,*N*′-dioxide **11** using 3-chloroperbenzoic acid (*m*-CPBA). This is followed by a one-pot Boekelheide rearrangement/nucleophilic substitution sequence to benzylic dibromide **12**.[17] After conversion of **12** to the *N*,*N*′-dioxide **13** using improved conditions (trifluoroacetic anhydride/urea hydrogen peroxide) for the oxidation of electron-poor pyridine derivatives,[18] cryptate **15** can be obtained under standard conditions (sodium template, high dilution) by macrocyclization reaction with aza-crown ether **14**.[19]

In our first approach to transform the methyl ester in **15** into a more suitable functional group for conjugation chemistry, we were able to saponify the ester using NaOH to the corresponding carboxylate in cryptate **16** (Scheme 2) in good

Scheme 2. Synthesis of Cryptates 16 and 5-Ln

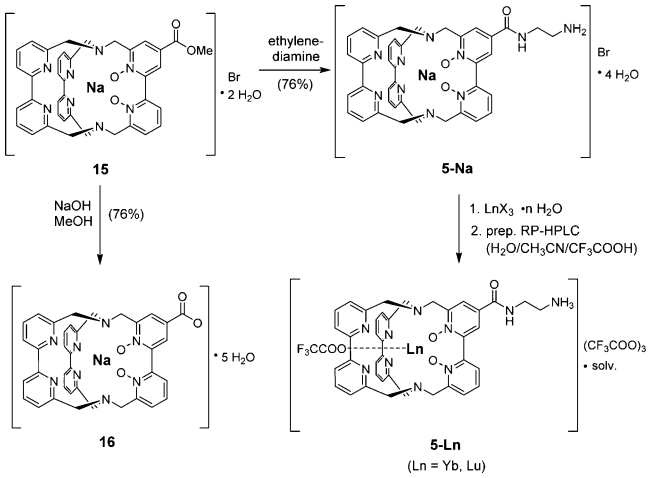

yield. Unfortunately, the carboxylate group proved to be a very sluggish reactant in peptide coupling reactions with primary amines under a variety of standard conditions (e.g., DCC/HOBt, HATU, PyBOP, etc). Because of these unexpected difficulties, we turned our attention to alternative transformations of the ester group of **15**. After a number of unsuccessful trials, we identified the reaction of **15** with an excess neat ethylene diamine to the corresponding amide **5-Na** as a very efficient way to generate a universally useful primary amine functionality for further conjugation chemistry (see analogy to cryptate **4-Ln** in Figure 2). Purification of this highly polar compound on a preparative scale is possible by column chromatography using silanized silica gel.

For the final complexation step, ytterbium was chosen as the paramagnetic center for a number of reasons: First, the analysis of its magnetic anisotropy is straightforward because of the known fact that ytterbium-induced NMR shifts in molecular complexes are overwhelmingly due to the dipolar, pseudocontact shift mechanism with only minor interference from corresponding contact shift contributions. This circumstance makes the magnetic analysis of **5-Yb** very convenient and the obtained results highly reliable. Second, we have already performed similar analyses of the magnetic anisotropies in the unfunctionalized cryptate **2-Yb** and similar species.[13d,e] Third and finally, ytterbium is not only relevant for its magnetic properties but it is also of considerable current interest in the emerging field of near-IR bioimaging because of its efficient luminescence in this spectral region.[20] In addition to the ytterbium cryptate **5-Yb**, the analogue **5-Lu** was also synthesized as a diamagnetic and photoinactive reference system. The metal exchange reaction of Ln^{3+} for Na^+ was performed similarly to the previously reported unfunctionalized cryptates **2-Ln** (Figure 1) but with the requirement for extended reaction times (t > 40 h). The crude lanthanoid cryptates with anions X^- (X = Cl, Br, or OTf) were purified by reversed-phase, preparative HPLC (H_2O+1 vol % CF_3COOH/CH_3CN). Under these harsh conditions, no decomposition of the cryptates was observed, which is an indication of the extremely high kinetic inertness of the complexes as has been seen before for similar cryptates.[11,13,15] The cryptate cations of **5-Ln** have most likely the inner-sphere composition shown in Figure 5. Because of the low pH (∼1) and the great excess of

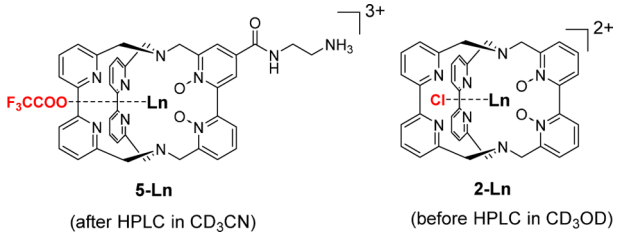

Figure 5. Composition of the inner coordination sphere of **2-Ln**[13d] and **5-Ln**.

trifluoroacetate anions in the HPLC eluent mixture, the obtained cryptates **5-Ln** are protonated at the primary amine and feature exclusively trifluoroacetate as the counteranions. From our previous studies on the corresponding unfunctionalized cryptates **2-Ln**, we know that there is exactly one available binding site in the inner coordination sphere of the lanthanoids. For example, if **2-Ln** is synthesized from $LnCl_3 \cdot 6H_2O$ and is not purified by HPLC, it features a chloride anion directly bound to the lanthanoid in methanolic solution (Figure 5, right).[13d] In the case of **5-Yb**, ^{19}F NMR in CD_3CN after HPLC purification shows two singlet resonances, one at −76.4 ppm and another at −116.5 ppm in an integrated ratio of 3:1. While the former signal is in the typical range for free trifluoroacetate anions,[21] we interpret the latter as originating from a paramagnetically shifted inner-sphere trifluoroacetate.

Chemical Structure in Solution—Nuclear Magnetic Resonance/Density Functional Theory. The investigations into the effects that structural variations of the core cryptate scaffold **2-Yb** have on the nature and spatial orientation of the corresponding magnetic anisotropy were performed by analyzing the lanthanoid-induced, paramagnetic ^1H NMR shifts. To assess these changes, we used the differences outlined in Figure 5, that is, the introduction of the peripheral functionalization in **5-Yb** resulting in the reduction of overall symmetry (from C_2 in **2-Yb** to C_1) and the exchange of a trifluoroacetate anion in **5-Yb** for the inner-sphere chlorido ligand in **2-Yb**. Both effects could potentially have an enormous impact on magnetic anisotropy as it has been documented recently in DOTA-derived systems.[9,10]

The ^1H NMR spectrum of **5-Yb** in CD_3CN (Figure 6b) shows a set of 29 paramagnetically shifted but very well-defined resonances corresponding to the immediate cryptate core structure (i.e., aromatic and benzylic hydrogen atoms in **5-Yb**). The signals for the C−H moieties in the peripheral ethylene diamine unit could not be identified unambiguously because of

DOI: 10.1021/acs.inorgchem.6b00591
Inorg. Chem. XXXX, XXX, XXX−XXX

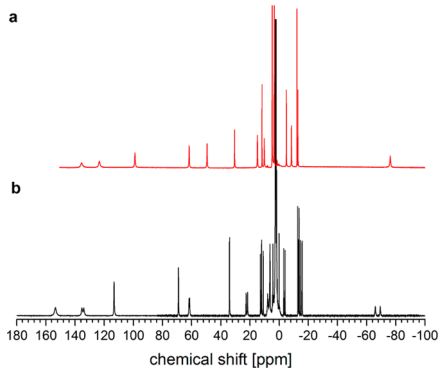

Figure 6. ^{1}H NMR spectra of (a) unfunctionalized **2-Yb** (CD_3OD, 400 MHz)[13d] with chloride in the inner coordination sphere and (b) functionalized **5-Yb** (CD_3CN, 500 MHz) with trifluoroacetate bound to the lanthanoid.

overlap with strong residual solvent signals. Overall, the spectral features are similar to the ones observed for **2-Yb** in CD_3OD (Figure 6a).[13d] Typically, signals that could be observed as singlets with an integral of two protons, in the case of **2-Yb**, split into two singlets for **5-Yb** with an integral of one proton each (see, e.g., the signals between −60 and −80 ppm in Figure 6). The shifts of the signals of the formerly equivalent protons show small separations, but the differences do not exceed 3.5 ppm. As in the case of the parent compound **2-Yb**, no exchange processes on the NMR time scale are observable for **5-Yb**.

Density functional theory (DFT) calculations in CH_3CN were performed on the cryptate cation of **5-Yb** to get a deeper understanding of the spatial structure of the cryptate. To keep the sizable computational demands as low as possible, we used a simplified model system with a water molecule bound to ytterbium instead of the actually present inner-sphere trifluoroacetate (cf. Figure 5). The obtained structure (Figure 7) shows great similarity to the calculated structure for **2-Yb**[13d]

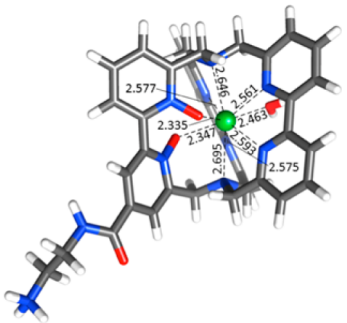

Figure 7. Calculated structure of **5-Yb** optimized in CH_3CN solution at the TPSSh/LCRECP/6-31G(d,p) level and bond distances of the metal coordination environment (Å).

(DFT) and the crystallographically determined one previously reported for the structurally related cryptate **2-Lu**.[13b] The optimized geometry for **5-Yb** retains a nearly undistorted, local C_2 symmetry in the immediate coordination sphere around the metal, where the symmetry axis contains the oxygen atoms of the coordinated water molecule and the Yb(III) ion. The general arrangement of the biaryl units remains virtually unaffected by the functionalization of the ligand.

Lanthanoid-Induced NMR Shift Analysis. The paramagnetic ^{1}H NMR shifts of the cryptate **5-Yb** were analyzed following the previously reported methodology,[13d,22] assuming that they are dominated by the pseudocontact contribution (δ^{pc}), which can be expressed as a linear combination of the five components of the magnetic susceptibility tensor χ:[23]

$$\delta^{pc} = \left(\chi_{zz} - \frac{1}{3}\mathrm{Tr}\chi\right)\left(\frac{3z^2 - r^2}{r^5}\right) + (\chi_{xx} - \chi_{yy})\left(\frac{x^2 - y^2}{r^5}\right) + \chi_{xy}\left(\frac{4E}{r^5}\right) + \chi_{xz}\left(\frac{4xz}{r^5}\right) + \chi_{yz}\left(\frac{4yz}{r^5}\right) \text{ with } r = \sqrt{x^2 + y^2 + z^2}$$

Here, x, y and z represent the Cartesian coordinates of the observed nuclei with the paramagnetic ion placed at the origin. In the principal magnetic axis system, the tensor is diagonalized, so that $\chi_{xy} = \chi_{xz} = \chi_{yz} = 0$. Thus, the pseudocontact shifts were analyzed by using a five-parameter least-squares search that minimizes the difference between the experimental and calculated pseudocontact shifts. These five parameters are ($\chi_{zz} - 1/3\mathrm{Tr}\chi$), ($\chi_{zz} - \chi_{yy}$), and a set of Euler angles that relate the principal magnetic axis system to the molecular coordinate system. Given the small chemical shift differences introduced by the absence of C_2-symmetry in **5-Yb**, we carried out this analysis using averaged chemical shifts (Table 1). The ^{1}H NMR chemical shifts of the unfunctionalized lutetium cryptate **2-Lu**[13d] were used to estimate the diamagnetic contributions. The DFT structure of **5-Yb** (Figure 7) optimized in acetonitrile solution provides very good agreement between the experimental and calculated Yb-induced shifts, with an agreement factor AF_j = 0.032 (Figure 8, Table 1). The excellent match between experiment and theory unambiguously proves that our DFT calculations provide a very accurate description of the

Table 1. Comparison of Experimental and Calculated ^{1}H NMR Shifts[a] for 5-Yb in Acetonitrile

proton	δ_i^{exp}	δ_i^{avg} [b]	$\delta_i^{avg,cald}$ [c]
H1o	−69.35/−65.97	−67.66	−68.46
H2o	21.63/22.55	22.09	25.89
H3o	12.79/10.88	11.84	12.73
H4o	0.02	0.02	2.11
H5o	−13.19/−14.55	−13.87	−13.96
H1b	153.49[d]	153.49	148.05
H2b	61.82/61.35	61.59	63.50
H3b	−3.18/-4.07	−3.63	−2.65
H4b	−12.82/-13.72	−13.27	−11.88
H5b	−15.59/-15.85	−15.72	−15.06
H6b	12.04/11.97	12.01	10.63
H7b	34.09/33.97	34.01	33.32
H8b	69.10/68.99	69.05	68.81
H9b	113.22[d]	113.22	114.63
H10b	135.27/133.96	134.62	137.96
AF_j [e]		0.0321	
$\chi_{zz} - \frac{1}{3}Tr\chi$		2740 ± 62	ppm Å^3
$\chi_{xx} - \chi_{yy}$		−8601 ± 138	ppm Å^3

[a]See Figure 8 for numbering scheme. [b]Averaged chemical shifts. [c]Values obtained from the analysis of the paramagnetic shifts assuming that the paramagnetic shifts are purely pseudocontact in origin. [d]Only one signal is observed. [e]$AF_j = [\sum_i (\delta_i^{exp} - \delta_i^{cal})^2 / \sum_i (\delta_i^{exp})^2]^{1/2}$, where δ_i^{exp} and δ_i^{exp} represent the experimental and calculated values of a nucleus i, respectively.

DOI: 10.1021/acs.inorgchem.6b00591
Inorg. Chem. XXXX, XXX, XXX−XXX

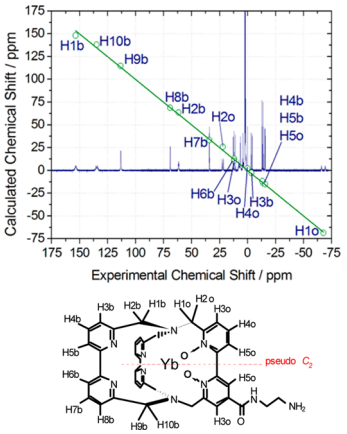

Figure 8. Experimental ^{1}H NMR spectrum (CD_3CN, 500 MHz) of **5-Yb**, plot of experimental versus calculated shifts, and numbering scheme for the hydrogen atoms in **5-Yb** (protons that would be related by the pseudo C_2 symmetry in the unfunctionalized cryptate have the same name). The solid line represents a perfect fit between experimental and calculated values.

structure of this complex, as much higher agreement factors $AF_j \approx 0.06-0.09$ have been considered to be acceptable for different nonaxial Yb(III) complexes.[24]

Magnetic Anisotropy. Multiple studies in the past have shown that magnetic anisotropy and hence the induced pseudocontact NMR shifts of Yb(III) complexes can be profoundly different upon subtle changes in the lanthanoid coordination environment.[9,10] For the purpose of this study, we can compare two factors governing the magnetic anisotropy in the related cryptates **2-Yb** and functionalized **5-Yb**, the reduction in symmetry from C_2 to C_1 and the exchange of inner-sphere monodentate ligands (Figure 5: chloride vs trifluoroacetate). As expected given the similarity of the measured chemical shifts of **2-Yb** and **5-Yb** (see Figure 6), the calculated axial ($\chi_{zz} - 1/3\mathrm{Tr}\chi$ = 2740 ppm Å^3) and rhombic ($\chi_{xx} - \chi_{yy}$ = −8601 ppm Å^3) components of the magnetic susceptibility tensor in **5-Yb** (Table 1) are very similar to those obtained previously for the unfunctionalized cryptate **2-Yb** ($\chi_{zz} - 1/3\mathrm{Tr}\chi$ = 2197 ppm Å^3; $\chi_{xx} - \chi_{yy}$ = −7916 ppm Å^3).[13d] Figure 9 shows a schematic representation of the core cryptate **5-Yb** surrounded by an isosurface of the induced pseudocontact shifts.

In addition to the size of the tensor components being similar in **2-Yb** and **5-Yb**, the relative spatial orientation of the two different tensors are also remarkably similar. Figure 10 clearly shows that the pseudocontact isosurfaces as a manifestation of the underlying tensors are almost indistinguishable apart from very small differences in size and virtually none in terms of orientation. This result underscores the very robust nature of the tensors in these cryptates with a remarkable degree of tolerance for functionalization and inner-sphere substitution of monodentate ligands.

Luminescence Properties. The unfunctionalized parent compound **2-Yb** has very favorable photoluminescence properties, especially after perdeuteration of the cryptand scaffold,[13b,d,e] which could be very interesting for bioanalytical applications using the new functionalized cryptates.[20] Therefore, we also measured the luminescence of **5-Yb** to see whether we could find any detrimental effect of functionalization on the photophysical properties. In the case of the indirect lanthanide sensitization via the surrounding organic ligand

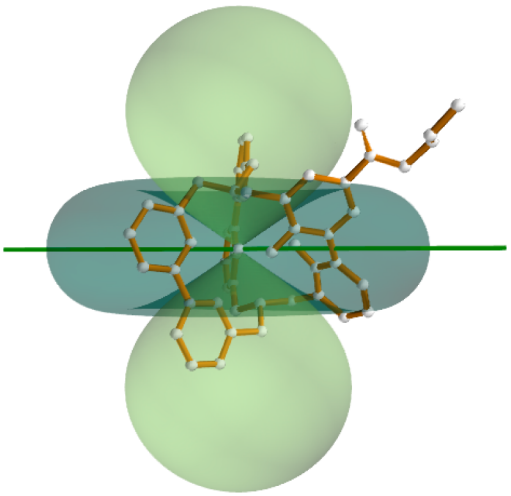

Figure 9. Graphical representation of **5-Yb** (without the bound water molecule) and the pseudocontact shift isosurface (light green: +12 ppm, dark green: −12 ppm; negative shifts correspond to shifts to lower field) corresponding to the magnetic susceptibility tensor χ. The green line illustrates the effective C_2 symmetry axis.[25]

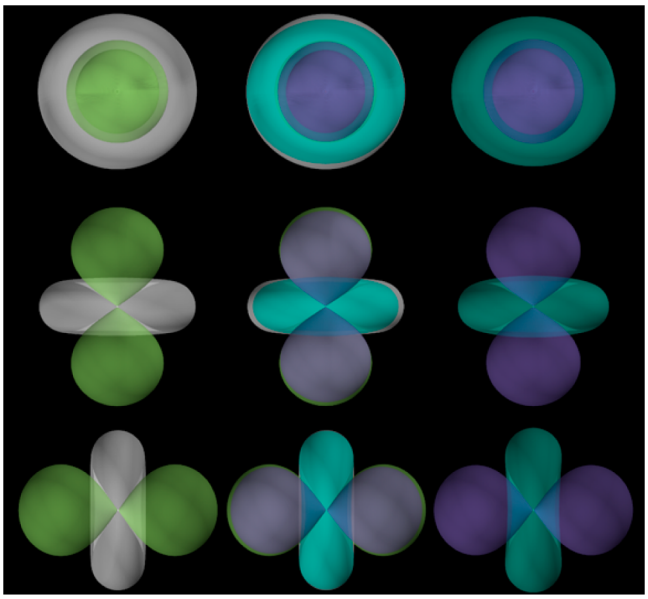

Figure 10. Graphical representation of the size and orientations of the pseudocontact shift isosurfaces of the functionalized and unfunctionalized cryptate along the three different Cartesian coordinate axes (rows) – Right column: **2-Yb**;[13d] Left column: **5-Yb**; Middle column: Overlay of **2-Yb** and **5-Yb**.

(antenna effect), the energy is usually transferred to the lanthanoid from the ligand-centered excited triplet level. From the low-temperature (77 K) steady-state emission spectrum of the photoinactive lutetium cryptate **5-Lu** (Figure 11), we could obtain an estimate for the zero-phonon $T_1 \rightarrow S_0$ transition energy $E(T_1) \approx 20\,400$ cm^{-1}, which is virtually identical to the values previously found for **2-Lu**[13b] and **2-Gd**.[26] Like **2-Yb**, functionalized **5-Yb** shows rather strong steady-state photoluminescence after excitation at λ_{ex} = 305 nm in CD_3OD (Figure 12) with an almost identical band shape of the transition $^2F_{5/2} \rightarrow {}^2F_{7/2}$ compared to the spectrum for **2-Yb**.[13c] In addition, the observed monoexponential luminescence decay (Figure 13) with a lifetime of τ_{obs} = 10.8 μs is also very similar

DOI: 10.1021/acs.inorgchem.6b00591
Inorg. Chem. XXXX, XXX, XXX−XXX

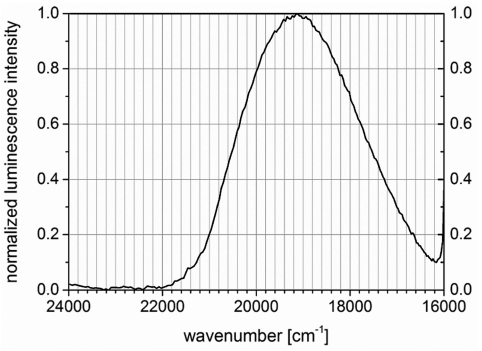

Figure 11. Low-temperature steady-state emission spectra (λ_{exc} = 315 nm, T = 77 K) for **5-Lu** in a glassy CH_3OH/EtOH matrix (1:1, v/v).

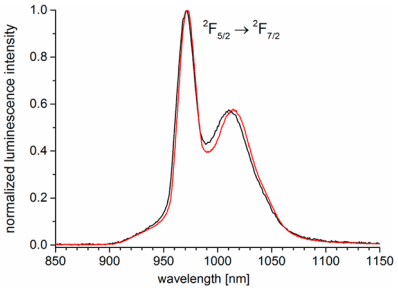

Figure 12. Normalized steady-state emission spectra for **5-Yb** (black) and for **2-Yb** (red)[13c] in solution (CD_3OD, λ_{exc} = 305 nm, emission path: long pass filter RG780).

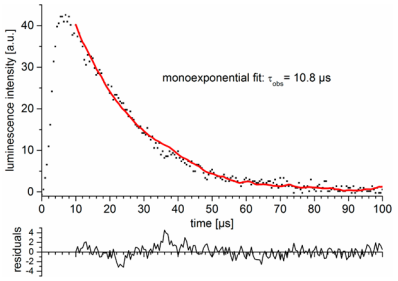

Figure 13. Luminescence decay profile of **5-Yb** (black) and monoexponential fit in red (CD_3OD, λ_{exc} = 305 nm, λ_{em} = 970 nm).

to the behavior observed for **2-Yb** (τ_{obs} = 12.3 μs) under identical conditions. Taken together, the excellent photoluminescence properties documented previously for the unfunctionalized cryptate **2-Yb** are completely retained in the functionalized cryptates **5-Yb**.

CONCLUSION

In summary, we have developed a practical synthetic route to rigid lanthanoid cryptates **5-Ln** (Ln = Yb, Lu) with a peripheral primary amino group for future conjugation chemistry to biomolecules. These species are highly stable in solution and can even be purified by reversed-phase HPLC. In addition, the functionalized ytterbium cryptate retains all excellent physical properties found in the unfunctionalized parent cryptate **2-Yb**, such as well-defined, time-invariant magnetic anisotropy and efficient photoluminescence in solution. Particularly remarkable is the great apparent resilience of its magnetic anisotropy toward changes in symmetry and anion exchange in the inner-coordination sphere. These findings show that this type of lanthanoid cryptate will be a very good candidate in future applications where stable magnetic properties are key and where DOTA-derived systems still suffer from fluxional magnetic behavior due to conformational and configurational exchange processes in the ligand backbone.

EXPERIMENTAL SECTION

General. Solvents were dried by standard procedures (tetrahydrofuran (THF), xylenes: Na; CH_2Cl_2; CaH_2), dry dimethylformamide (DMF) was used as purchased. Air-sensitive reactions were performed under a dry, dioxygen-free atmosphere of N_2 using Schlenk technique. Column chromatography was performed with silica gel 60 (Merck KGaA, 0.063−0.200 mm) or for cryptate **5-Na** with silanized silica gel 60 (Merck KGaA, 0.063−0.200 mm). Analytical thin layer chromatography (TLC) was done on silica gel 60 F_{254} plates (Merck, coated on aluminum sheets). Electrospray ionization (ESI) mass spectrometry was measured using Bruker Daltonics Esquire 3000plus or Bruker Daltonics APEX II FT-ICR (FAB). NMR spectra were measured on a Bruker AVII+500 (^{1}H: 500 MHz), AVII+400 (^{1}H: 400 MHz), DPX-250 (^{1}H: 250 MHz, ^{13}C: 62.9 MHz), and DPX-200 (^{1}H: 200 MHz, ^{13}C: 50 MHz).

Density Functional Theory Calculations. All calculations were performed employing DFT within the hybrid meta generalized gradient approximation, with the TPSSh exchange-correlation functional,[27] and the Gaussian 09 package (Revision D.01).[28] Full geometry optimizations of **5-Yb** were performed in acetonitrile solution by using the large-core relativistic effective core potential (LCRECP) of Dolg et al. and the related [5s4p3d]-GTO valence basis set for Yb,[29] and the standard 6-31G(d,p) basis set for C, H, N, and O atoms. No symmetry constraints were imposed during the optimizations. The default values for the integration grid ("fine") and the self-consistent field energy convergence criteria (1×10^{-8}) were used. The stationary points found on the potential energy surfaces as a result of the geometry optimizations were tested to represent energy minima rather than saddle points via frequency analysis. Solvent effects (acetonitrile) were taken into account by using the integral equation formalism variant of the polarizable continuum model as implemented in Gaussian 09.[30]

Luminescence Spectroscopy. Steady-state emission spectra were acquired on a PTI Quantamaster QM4 spectrofluorimeter using 1.0 cm quartz cuvettes. The excitation light source was a 75 W continuous xenon short arc lamp. Emission was monitored at 90° using a PTI P1.7R detector module (Hamamatsu PMT R5509−72 with a Hamamatsu C9525 power supply operated at −1500 V and a Hamamatsu liquid N_2 cooling unit C9940 set to −80 °C). For the near-IR steady-state emission measurements, a long-pass filter RG-780 (Schott, 3.0 mm thickness, transmission >83% between 800 and 850 nm and >99% between 850 and 1700 nm) was used in the emission channel to avoid higher-order excitation light. Low-temperature spectra were recorded on frozen glasses of solutions of **5-Lu** (MeOH/EtOH 1:1, v/v) using a dewar cuvette filled with liquid N_2 (T = 77 K). Spectral selection was achieved by single grating monochromators (excitation: 1200 grooves/mm, blazed at 300 nm; near-IR emission: 600 grooves/mm, blazed at 1200 nm). Luminescence lifetimes were determined with the same instrumental setup without the use of the long-pass filter. The light source for these measurements was a xenon flash lamp (Hamamatsu L4633; 10 Hz repetition rate, pulse width ca. 1.5 μs full width at half-maximum). Lifetime data analysis (deconvolution, statistical parameters, etc.) was performed using the software package FeliX32 from PTI. Lifetimes were determined by deconvolution fitting of the decay profiles with the instrument response function, which was determined using a dilute aqueous dispersion of colloidal silica (Ludox AM-30). The estimated uncertainties in τ are ±10%.

Synthesis. *6,6′-Dimethyl-2,2′-bipyridine-4-carboxylic Acid Methyl Ester (**10**).* Under N_2, a two-neck Schlenk flask equipped with a reflux condenser was charged with 2-methyl-6-(trifluoromethylsulfonyloxy)-isonicotinic acid methyl ester (**9**)[16] (11.97 g, 40.00 mmol, 1.0 equiv), 2-methyl-6-(tributylstannyl)pyridin (**8**)[16] (15.29 g, 40.00 mmol, 1.0 equiv), and PPh_3 (1.05 g, 4.00 mmol, 0.1 equiv) in dry

DOI: 10.1021/acs.inorgchem.6b00591
Inorg. Chem. XXXX, XXX, XXX−XXX

xylene (300 mL, isomeric mixture). The solution was degassed by one freeze−pump−thaw cycle before solid $[PdCl_2(PPh_3)_2]$ (1.40 g, 2.00 mmol, 0.05 equiv) was added. After two additional freeze−pump−thaw cycles, the yellow suspension was heated to reflux for 24 h. The reaction mixture was allowed to come to ambient temperature and was poured into a saturated, aqueous solution of Na_2H_2EDTA (300 mL). The aqueous phase was extracted with CH_2Cl_2 (3 × 300 mL), and the combined organic phases were dried ($MgSO_4$) and concentrated under reduced pressure. The remaining residue was dissolved in CH_3CN, and the solution was extracted continuously in a liquid−liquid extractor with *n*-heptane for 24 h. The pale yellow product, which crystallized from the extract after standing overnight at room temperature, was collected, washed with *n*-heptane, and dried in vacuo (6.78 g, 70%). The analytical data were in complete agreement with the literature.[14,16]

^{1}H NMR (200 MHz, $CDCl_3$): δ = 8.72 (s, 1 H), 8.20 (d, J = 7.8 Hz, 1 H), 7.71 (s, 1 H), 7.68 (d, J = 7.8 Hz, 1 H), 7.18 (d, J = 7.8 Hz, 1 H), 3.98 (s, 3 H), 2.72 (s, 3 H), 2.69 (s, 3 H) ppm.

*6,6′-Dimethyl-4-methyloxycarbonyl-2,2′-bipyridine N,N′-dioxide (**11**).* With cooling in an ice bath, a solution of *m*-chloroperoxybenzoic acid (32.35 g of 77 wt %, 24.90 g of pure, 144 mmol, 2.4 equiv) in CH_2Cl_2 (750 mL) was added dropwise to a solution of 6,6′-dimethyl-2,2′-bipyridine-4-carboxylic acid methyl ester (**10**) (14.57 g, 60.1 mmol, 1.0 equiv) in CH_2Cl_2 (600 mL) over the course of 1.5 h. The pale yellow solution was allowed to reach room temperature over ca. 3 h and was stirred overnight. After extraction of the reaction mixture with aq. $NaHCO_3$ solution (pH 8, 2 × 300 mL) and water (300 mL), the organic layer was dried over $MgSO_4$, and the solvent was removed under reduced pressure (bath temperature <35 °C). The crude product was purified by column chromatography (SiO_2, CH_2Cl_2/MeOH 100:1 → 24:1) to afford the title compound as an off-white solid (13.85 g, 84%).

^{1}H NMR (250 MHz, $CDCl_3$): δ = 8.01 (br s, 2 H), 7.49−7.30 (m, 3 H), 3.94 (s, 3 H), 2.64 (s, 3 H), 2.61 (s, 3 H) ppm. ^{13}C NMR (62.9 MHz, $CDCl_3$): δ = 164.1, 150.2, 150.0, 143.7, 143.2, 127.3, 126.8, 125.7, 125.5, 125.3, 124.9, 52.7, 17.97, 17.94. MS (FAB, pos. mode): m/z (%) = 275.1 (100, $[M + H]^+$), 259.1 (13). TLC: R_f = 0.08 (SiO_2, CH_2Cl_2/MeOH 24:1, detection: UV). mp:190−192 °C (decomp).

*6,6′-Bis(bromomethyl)-2,2′-bipyridine-4-carboxylic Acid Methyl Ester (**12**).*[17] Under N_2, $(CF_3CO)_2O$ (44.1 mL, 66.6 g, 317 mmol, 12 equiv) was added dropwise via syringe to a yellow solution of **11** (7.25 g, 26.4 mmol, 1.0 equiv) in dry CH_2Cl_2 (80 mL). The brown reaction mixture was heated under reflux for 1.5 h before the volatiles were removed in vacuo. Under N_2, the obtained orange residue was dissolved in a mixture of dry DMF/THF (40 mL, 1:1, v/v). Under N_2 and with ice-cooling, anhydrous LiBr (18.4 g, 211 mmol, 8.0 equiv) was dissolved in dry THF (50 mL), and the cold solution was added dropwise to the reaction mixture. After it was stirred at room temperature for 12 h, the solvents were removed under reduced pressure (bath temperature 40 °C). The brown residue was dissolved in CH_2Cl_2/water (400 mL, 1:1, v/v), and the aqueous phase was adjusted to pH ≈ 6 with saturated aqueous Na_2CO_3. The organic layer was washed with additional water (2 × 150 mL), dried ($MgSO_4$), and concentrated to dryness. The crude product was purified by column chromatography (SiO_2, CH_2Cl_2/MeOH 100:1, preloading onto SiO_2) to give the product as a yellow solid (7.00 g, 66%).

^{1}H NMR (200 MHz, $CDCl_3$): δ = 8.97−8.84 (m, 1 H), 8.47−8.33 (m, 1 H), 8.08−7.96 (m, 1 H), 7.90 (t, J = 7.8 Hz, 1 H), 7.59−7.47 (m, 1 H), 4.73 (s, 2 H), 4.69 (s, 2 H), 4.02 (s, 4 H) ppm. ^{13}C NMR (50 MHz, $CDCl_3$): δ = 165.4, 157.6, 156.6, 156.4, 154.4, 139.9, 138.5, 124.4, 123.1, 121.0, 120.2, 53.0, 33.6, 33.4 ppm. MS (ESI, pos. mode): m/z (%) 258.99 (42), 336.88 (46), 400.74 (100, $[M + H]^+$), 422.69 (100, $[M + K]^+$). TLC: R_f = 0.64 (SiO_2, CH_2Cl_2/MeOH 100:1, detection UV).

*6,6′-Bis(bromomethyl)-4-methyloxycarbonyl-2,2′-bipyri-dine N,N′-dioxide (**13**).*[18] Under N_2 and with cooling in an ice bath, urea/H_2O_2 adduct (3.77 g, 40.1 mmol, 2.3 equiv) was added in portions to a suspension of **3** (6.97 g, 17.4 mmol, 1.0 equiv) in dry CH_2Cl_2 (300 mL). Then, $(CF_3CO)_2O$ (5.6 mL, 8.42 g, 40.1 mmol, 2.3 equiv) was added slowly; the mixture was allowed to warm to room temperature and stirred overnight (15 h). A saturated solution of sodium thiosulfate pentahydrate (10 mL) and water (200 mL) was added, and the mixture was stirred for 30 min. The phases were separated, and the aqueous phase was extracted with CH_2Cl_2 (2 × 75 mL). The combined organic layers were dried ($MgSO_4$) and concentrated. The isolated crude product was purified by column chromatography (SiO_2, CH_2Cl_2/MeOH 100:1 → 25:1, preloading onto SiO_2) to give the title compound as a colorless solid (5.85 g, 78%).

^{1}H NMR (200 MHz, $CDCl_3$): δ = 8.23 (d, J = 2.5 Hz, 1 H), 8.14 (d, J = 2.4 Hz, 1 H), 7.67 (dd, J = 2.0, 7.5 Hz, 1 H), 7.59−7.50 (m, 1 H), 7.34 (t, J = 7.9 Hz, 1 H), 4.73 (s, 2 H), 4.70 (s, 2 H), 3.96 (s, 3 H) ppm. ^{13}C NMR (126 MHz, $CDCl_3$): δ = 163.7, 148.4, 148.2, 143.6, 142.7, 128.0, 127.9, 127.8, 127.5, 125.3, 124.7, 53.1, 25.4, 25.1 ppm. MS (ESI^+): m/z (%) = 454.73 (100, $[M + Na]^+$, Br_2-pattern). TLC: R_f = 0.22 (SiO_2, CH_2Cl_2/MeOH 25:1, detection: UV).

*Sodium Cryptate **15**.* Under N_2, macrocycle **14**[19] (0.48 g, 1.22 mmol, 1.0 equiv) and the dibromide **13** (0.53 g, 1.22 mmol, 1.0 equiv) were dissolved in CH_3CN (500 mL, HPLC grade), and Na_2CO_3 (1.29 g, 12.2 mmol, 10 equiv) was added. The mixture was heated under reflux for 40 h, cooled to ambient temperature, and filtered. The filtrate was concentrated under reduced pressure, and the resulting residue was subjected to column chromatography (SiO_2, gradient: CH_2Cl_2/MeOH 15:1 → 9:1) to yield the title compound as a light-yellow solid (0.30 g, 31%).

^{1}H NMR (200 MHz, $CDCl_3$): δ = 8.26−8.18 (m, 1 H), 8.10−8.02 (m, 1 H), 8.01−7.92 (m, 1 H), 7.88−7.60 (m, 8 H), 7.58−7.33 (m, 4 H), 4.32 (d, J = 12.0 Hz, 1 H), 4.29 (d, J = 11.7 Hz, 1 H), 4.08−3.31 (m, 13 H) ppm. ^{13}C NMR (50.3 MHz, $CDCl_3$): δ = 163.6, 158.8, 158.4 157.8, 157.6, 157.1, 157.0, 156.4, 156.2, 148.6, 148.5, 145.5, 144.0, 138.32, 138.30, 130.2, 128.6, 126.9, 126.8, 125.4, 125.3, 124.74, 124.68, 122.2, 122.1, 121.3, 121.2, 60.9, 60.70, 60.66, 60.62, 54.6, 54.3, 53.1 ppm. MS (ESI, pos. mode): m/z (%) = 687.20 (100, $[M]^+$).TLC: R_f = 0.45 (SiO_2, CH_2Cl_2/MeOH 9:1, detection UV + I_2 vapor). Anal. Calcd (Found) for $C_{38}H_{32}BrN_8NaO_4 \cdot 2\,H_2O$ (M_r = 803.64): C, 56.79 (56.61); H, 4.52 (4.28); N, 13.94 (13.73).

*Sodium Cryptate **16**.* Compound **15** (71.0 mg, 88.3 μmol, 1.0 equiv) was dissolved in MeOH (8 mL), and a solution of NaOH (18.5 mg, 462 μmol, 5.2 equiv) in water (2 mL) was added dropwise. The solution was stirred at 40 °C (bath temperature) for 3 h. The solvents were removed, and the residue was subjected to column chromatography (SiO_2, CH_2Cl_2/MeOH 2:1, detection: UV). The product was obtained as a colorless solid (51 mg, 76%).

^{1}H NMR (200 MHz, CD_3OD): δ = 8.22 (d, J = 2.3 Hz, 1 H), 8.14 (d, J = 2.3 Hz, 1 H), 7.99−7.73 (m, 10 H), 7.66−7.36 (m, 5 H), 4.30 (d, J = 11.8 Hz, 2 H), 3.95−3.75 (m, 4 H), 3.64−3.34 (m, 6 H) ppm. ^{13}C NMR (50.3 MHz, CD_3OD): δ = 169.5, 160.1, 159.3, 159.2, 157.91, 157.88, 150.2, 149.5, 146.6, 145.9, 139.5, 139.3, 131.0, 130.6, 128.5, 128.4, 128.1, 125.61, 125.56, 125.51, 123.13. 123.11, 122.34, 122.31, 61.81, 61.73, 61.69, 55.63, 55.55 ppm. MS (ESI, pos. mode): m/z (%) = 673.21 (66, $[M + H]^+$), 695.17 (100, $[M + Na]^+$). R_f = 0.17 (SiO_2, CH_2Cl_2/MeOH 2:1, detection: UV). Anal. Calcd (Found) for $C_{37}H_{29}N_8NaO_4 \cdot 5H_2O$ (M_r = 762.74): C, 58.26 (57.96); H, 5.15 (4.94); N, 14.69 (14.72).

*Sodium Cryptate **5-Na**.* Under N_2 and with ice-cooling, **15** (250.7 mg, 0.327 mmol, 1.0 equiv) was added as a solid to freshly dried and distilled ethylenediamine (3.5 mL, 3.15 g, 52.4 mmol, 150 equiv). The slightly red suspension was allowed to warm to room temperature and stirred for 2 d before the volatiles were removed in vacuo. The crude product was subjected to column chromatography (silanized SiO_2, CH_2Cl_2/MeOH 24:1, preloading onto silanized SiO_2) to give pure **5-Na** as an off-white solid (197 mg, 76%).

^{1}H NMR (250 MHz, CD_3OD): δ = 8.48 (d, J = 2.3 Hz, 1 H), 8.35 (d, J = 2.6 Hz, 1 H), 7.96−7.82 (m, 9 H), 7.79 (dd, J = 2.0, 7.8 Hz, 1 H), 7.62−7.53 (m, 1 H), 7.51−7.42 (m, 4 H), 4.43−4.30 (m, 2 H), 4.02−3.85 (m, 4 H), 3.83−3.60 (m, 4 H), 3.59−3.39 (m, 4 H), 3.30−3.20 (m, 2 H) ppm. ^{13}C NMR (62.9 MHz, CD_3OD): δ = 166.3, 160.1, 159.3, 159.2, 158.3, 157.8, 150.25, 150.23, 146.2, 146.0, 139.6, 139.4, 131.9, 131.4, 128.71, 128.69, 126.8, 125.7, 123.2, 122.4, 61.9, 61.82, 61.75, 61.6, 55.5, 55.4, 41.0, 39.4 ppm. MS (ESI, pos. mode): m/z (%) 357.99 (34), 715.10 (100, $[M]^+$). Anal. Calcd (Found) for

DOI: 10.1021/acs.inorgchem.6b00591
Inorg. Chem. XXXX, XXX, XXX−XXX

$C_{39}H_{36}BrN_{10}NaO_3 \cdot 4\ H_2O$ (M_r = 867.72): C, 53.98 (53.85); H, 5.11 (4.92); N, 16.14 (16.00). TLC: R_f = 0.48 (SiO_2, CH_2Cl_2/MeOH 4:1, detection UV + ninhydrin).

Synthesis of Ln Complexes ***5-Ln****—General Procedure.* The sodium cryptate **5-Na** (1.0 equiv) and $Ln(X)_3 \cdot nH_2O$ (1.7 equiv) were suspendend in CH_3CN (HPLC grade), and the mixture was heated under reflux for at least 40 h. The solvent was removed in vacuo, and the remaining residue was taken up in a minimum of CH_3CN/H_2O (1:1, v/v) and subjected to preparative reversed-phase HPLC (Lichrospher RP-18e, 250× 10 mm-10 μm, flow rate: 3.0 mL min^{-1}, UV detection: 300 nm) with H_2O (+1% TFA, v/v) as mobile Phase A, CH_3CN (HPLC grade) as mobile Phase B, and the following gradient: 0 min: 85%A/15%B; 5 min 85%A/15%B; 19 min: 45%A/55%B; 25 min: 45%A/55%B; 40 min: 85%A/15%B; 50 min: 85%A/15%B.

The composition of the collected fractions was checked by analytical, reversed-phase HPLC (Lichrospher RP-18e, 125 × 4 mm-5 μm, flow rate: 1 mL min^{-1}, UV detection: 300 nm), using the same mobile phase mixture and gradient (see Supporting Information for HPLC traces). Fractions containing pure lanthanoid complexes **5-Ln** were combined (retention times $t_r \approx$ 12.6−12.7 min) and evaporated to dryness at room temperature. The complexes were isolated as off-white or faintly yellow solids.

Ytterbium Cryptate ***5-Yb****.* **5-Na** (30 mg, 38 μmol, 1.0 equiv) and $YbCl_3 \cdot 6\ H_2O$ (25 mg, 63 μmol, 1.7 equiv) in 15 mL of CH_3CN (HPLC grade). Yield: 14 mg.

^{1}H NMR (500 MHz, CD_3CN): δ = 153.5 (H1b, 2 H), 135.3/134.0 (H10b, 2 H), 113.2 (H9b, 2 H), 69.1/69.0 (H8b, 2 H), 61.8/61.4 (H2b, 2 H), 34.1/33.9 (H7b, 2H), 22.6/21.6 (H2o, 2H), 12.8/10.9 (H3o, 2 H), 12.04/11.97 (H6b, 2 H), 0.02 (H4o, 1 H), −3.2/−4.1 (H3b, 2 H), −12.8/−13.7 (H4b, 2 H), −13.2/−14.6 (H5o, 2 H), −15.6/−15.9 (H5b, 2 H), −66.0/−69.4 (H1o, 2H) ppm. Remarks: (a) The signals representing the four protons of the ethylene group could not be identified unambigiously, as in the respective region of the spectrum there are several solvent signals; (b) The numbering scheme uses the same name for protons that would be symmetry-related in the unfunctionalized cryptate, see Figure 8. ^{19}F NMR (376 MHz, CD_3CN): δ = −76.4 (s, 9 F), −116.5 (s, 3 F) ppm. ^{19}F NMR (376 MHz, CD_3OD): δ = −77.0 (s, 9 F), −114.4 (s, 3 F) ppm. MS (ESI, pos. mode): *m*/*z* (%) = 489.7 (100, $\{[Yb(II)(L)] + CF_3COO\}^{2+}$), 560.8 (58). Analytical HPLC: t_r = 12.7 min (see Figure S13 in the Supporting Information).

Lutetium Cryptate ***5-Lu****.* **5-Na** (20 mg, 25 μmol, 1.0 equiv) and $Lu(OTf)_3$ (27 mg, 43 μmol, 1.7 equiv) in 15 mL of CH_3CN (HPLC grade). Yield: 18 mg.

^{1}H NMR (400 MHz, CD_3CN): δ = 10.0 (t, *J* = 4.6 Hz, 1 H), 8.90 (d, *J* = 2.3 Hz, 1 H), 8.70 (d, *J* = 2.4 Hz, 1 H), 8.48 (dd, *J* = 1.7, 7.8 Hz, 1 H), 8.33−8.28 (m, 2 H), 8.23−8.05 (m, 8 H), 7.62−7.55 (m, 4 H), 4.79−4.71 (m, 4 H), 4.13−3.93 (m, 6 H), 3.84 (d, *J* = 13.1 Hz, 1 H), 3.80−3.64 (m, 5 H), 3.23 (t, *J* = 5.3 Hz, 2 H) ppm. MS (ESI, pos. mode.): *m*/*z* (%) = 360. (87), 478.3 (79), 561.3 (84), 697.3 (100). Analytical HPLC: t_r = 12.6 min (see Figure S14 in the Supporting Information).

■ ASSOCIATED CONTENT

Supporting Information

The Supporting Information is available free of charge on the ACS Publications website at DOI: 10.1021/acs.inorgchem.6b00591.

NMR spectra of the compounds **10**, **11**, **12**, **13**, **15**, **16**, **5-Na**, and **5-Lu**. HPLC traces for **5-Ln**. Cartesian coordinates for the structure of **5-Yb** as obtained by DFT calculations. (PDF)

■ AUTHOR INFORMATION

Corresponding Authors

*E-mail: michael.seitz@uni-tuebingen.de. (M.S.)

*E-mail: carlos.platas.iglesias@udc.es. (C.P.-I.)

Notes

The authors declare no competing financial interest.

■ ACKNOWLEDGMENTS

Financial support is gratefully acknowledged from DFG (Emmy Noether and Heisenberg Fellowships for M.S., Research Grant SE 1448/6-1), German National Academic Foundation (predoctoral fellowship for E.K.), and Int. Max Planck Research School in Chemical Biology (predoctoral fellowship for C.B.). C.P.-I. thanks Centro de Supercomputación de Galicia (CESGA) for providing the computer facilities.

■ REFERENCES

(1) *The Rare Earth Elements - Fundamentals and Applications;* Atwood, D. A., Ed.; Wiley: Chichester, U.K., 2012.

(2) Geraldes, C. F. G. C. Lanthanide Shift Reagents. In *The Rare Earth Elements - Fundamentals and Applications;* Atwood, D. A., Ed.; Wiley: Chichester, U.K., 2012; p 501.

(3) *The Chemistry of Contrast Agents in Medical Magnetic Resonance Imaging,* 2nd ed.; Merbach, A. S., Helm, L., Toth, E., Eds.; Wiley: Chichester, U.K., 2013.

(4) (a) Habib, F.; Murugesu, M. *Chem. Soc. Rev.* **2013**, *42*, 3278. (b) Woodruff, D. N.; Winpenny, R. E. P.; Layfield, R. A. *Chem. Rev.* **2013**, *113*, 5110. (c) Liddle, S. T.; van Slageren, J. *Chem. Soc. Rev.* **2015**, *44*, 6655.

(5) (a) Su, X.-C.; Otting, G. *J. Biomol. NMR* **2010**, *46*, 101. (b) Otting, G. *Annu. Rev. Biophys.* **2010**, *39*, 387. (c) Liu, W.-M.; Overhand, M.; Ubbink, M. *Coord. Chem. Rev.* **2014**, *273*−*274*, 2.

(6) Selected review: Stasiuk, G. J.; Long, N. J. *Chem. Commun.* **2013**, *49*, 2732 and references cited therein..

(7) Selected reviews: (a) Parker, D.; Dickins, R. S.; Puschmann, H.; Crossland, C.; Howard, J. A. K. *Chem. Rev.* **2002**, *102*, 1977. (b) Platas-Iglesias, C. *Eur. J. Inorg. Chem.* **2012**, *2012*, 2023.

(8) Selected examples: (a) Martins, A. F.; Eliseeva, S. V.; Carvalho, H. F.; Teixeira, J. M. C.; Paula, C. T. B.; Hermann, P.; Platas-Iglesias, C.; Petoud, S.; Toth, E.; Geraldes, C. F. G. C. *Chem. - Eur. J.* **2014**, *20*, 14834. (b) Polasek, M.; Rudovsky, J.; Hermann, P.; Lukes, I.; Vander Elst, L.; Muller, R. N. *Chem. Commun.* **2004**, 2602. (c) Keizers, P. H. J.; Desreux, J. F.; Overhand, M.; Ubbink, M. *J. Am. Chem. Soc.* **2007**, *129*, 9292.

(9) (a) Boulon, M.-E.; Cucinotta, G.; Luzon, J.; Degl'Innocenti, C.; Perfetti, M.; Bernot, K.; Calvez, G.; Caneschi, A.; Sessoli, R. *Angew. Chem., Int. Ed.* **2013**, *52*, 350. (b) Cucinotta, G.; Perfetti, M.; Luzon, J.; Etienne, M.; Car, P. E.; Caneschi, A.; Calvez, G.; Bernot, K.; Sessoli, R. *Angew. Chem., Int. Ed.* **2012**, *51*, 1606.

(10) (a) Blackburn, O. A.; Chilton, N. F.; Keller, K.; Tait, C. E.; Myers, W. K.; McInnes, E. J. L.; Kenwright, A. M.; Beer, P. D.; Timmel, C. R.; Faulkner, S. *Angew. Chem., Int. Ed.* **2015**, *54*, 10783. (b) Liu, T.; Nonat, A.; Beyler, M.; Regueiro-Figueroa, M.; Nchimi Nono, K.; Jeannin; Camerel, O. F.; Debaene, F.; Cianférani-Sanglier, S.; Tripier, R.; Platas-Iglesias, C.; Charbonnière, L. J. *Angew. Chem., Int. Ed.* **2014**, *53*, 7259. (c) Blackburn, O. A.; Edkins, R. M.; Faulkner, S.; Kenwright, A. M.; Parker, D.; Rogers, N. J.; Shuvaev, S. *Dalton Trans.* **2016**, *45*, 6782.

(11) Review: Zwier, J. M.; Bazin, H.; Lamarque, L.; Mathis, G. *Inorg. Chem.* **2014**, *53*, 1854.

(12) Alpha, B.; Lehn, J.-M.; Mathis, G. *Angew. Chem., Int. Ed. Engl.* **1987**, *26*, 266.

(13) (a) Lehn, J.-M.; Roth, C. O. *Helv. Chim. Acta* **1991**, *74*, 572. (b) Doffek, C.; Alzakhem, N.; Molon, M.; Seitz, M. *Inorg. Chem.* **2012**, *51*, 4539. (c) Doffek, C.; Seitz, M. *Angew. Chem., Int. Ed.* **2015**, *54*, 9719. (d) Doffek, C.; Alzakhem, N.; Bischof, C.; Wahsner, J.; Güden-Silber, T.; Lügger, J.; Platas-Iglesias, C.; Seitz, M. *J. Am. Chem. Soc.* **2012**, *134*, 16413. (e) Güden-Silber, T.; Doffek, C.; Platas-Iglesias, C.; Seitz, M. *Dalton Trans.* **2014**, *43*, 4238.

DOI: 10.1021/acs.inorgchem.6b00591
Inorg. Chem. XXXX, XXX, XXX−XXX

(14) (a) Havas, F.; Danel, M.; Galaup, C.; Tisnes, P.; Picard, C. *Tetrahedron Lett.* **2007**, *48*, 999. (b) Havas, F.; Leygue, N.; Mestre, B.; Galaup, C.; Picard, C. *Tetrahedron* **2009**, *65*, 7673.
(15) (a) Lamarque, L.; Bazin, H.; Blanche, E. (Cisbio International). Patent WO 2010/070232, June 24, 2010. (b) Ansanay, H.; Fink, M.; Mathis, G.; Maurel, D.; Trinquet, E.; Pin, J.-P. (Cisbio International). Patent WO 2006/085040, August 17, 2006.
(16) Mathieu, J.; Marsura, A. *Synth. Commun.* **2003**, *33*, 409.
(17) In analogy to: Psychogios, N.; Regnouf-de-Vains, J.-B.; Stoeckli-Evans, H. M. *Eur. J. Inorg. Chem.* **2004**, *2004*, 2514.
(18) In analogy to: Caron, S.; Do, N. M.; Sieser, J. E. *Tetrahedron Lett.* **2000**, *41*, 2299.
(19) Newkome, G. R.; Pappalardo, S.; Gupta, V. K.; Fronczek, F. R. *J. Org. Chem.* **1983**, *48*, 4848.
(20) Selected reviews: (a) Bünzli, J.-C. G. *J. Lumin.* **2016**, *170*, 866. (b) Bünzli, J.-C. G.; Eliseeva, S. V. *J. Rare Earths* **2010**, *28*, 824. (c) Comby, S.; Bünzli, J.-C. G. In *Handbook on the Physics and Chemistry of Rare Earths;* Gschneidner, K. A., Jr., Bünzli, J.-C. G., Pecharsky, V. K., Eds.; Elsevier: Amsterdam, 2007; Vol. 37, pp 217.
(21) Emsley, J. W.; Phillips, L. *Prog. Nucl. Magn. Reson. Spectrosc.* **1971**, *7*, 1.
(22) Rodríguez-Rodríguez, A.; Esteban-Gómez, D.; de Blas, A.; Rodríguez-Blas, T.; Fekete, M.; Botta, M.; Tripier, R.; Platas-Iglesias, C. *Inorg. Chem.* **2012**, *51*, 2509.
(23) Forsberg, J. H.; Delaney, R. M.; Zhao, Q.; Harakas, G.; Chandran, R. *Inorg. Chem.* **1995**, *34*, 3705.
(24) Lisowski, J.; Sessler, J. L.; Lynch, V.; Mody, T. D. *J. Am. Chem. Soc.* **1995**, *117*, 2273. (b) Lima, L. M. P.; Lecointre, A.; Morfin, J.-F.; de Blas, A.; Visvikis, D.; Charbonnière, L. J.; Platas-Iglesias, C.; Tripier, R. *Inorg. Chem.* **2011**, *50*, 12508. (c) del C. Fernández-Fernández, M.; Bastida, R.; Macías, A.; Pérez-Lourido, P.; Platas-Iglesias, C.; Valencia, L. *Inorg. Chem.* **2006**, *45*, 4484.
(25) Graphical representation calculated using the program Mayavi 2: Ramachandran, P.; Varoquaux, G. *Comput. Sci. Eng.* **2011**, *13*, 40.
(26) Prodi, L.; Maestri, M.; Balzani, V.; Lehn, J.-M.; Roth, C. *Chem. Phys. Lett.* **1991**, *180*, 45.
(27) Tao, J. M.; Perdew, J. P.; Staroverov, V. N.; Scuseria, G. E. *Phys. Rev. Lett.* **2003**, *91*, 146401.
(28) Frisch, M. J. et al. *Gaussian 09,* Revision D.01; Gaussian, Inc: Wallingford, CT, 2009.
(29) Dolg, M.; Stoll, H.; Savin, A.; Preuss, H. *Theor. Chim. Acta* **1989**, *75*, 173.
(30) Tomasi, J.; Mennucci, B.; Cammi, R. *Chem. Rev.* **2005**, *105*, 2999.

DOI: 10.1021/acs.inorgchem.6b00591
Inorg. Chem. XXXX, XXX, XXX−XXX